Unoccupied Aerial Systems-based Disease Assessments of Specialty Crops: Case Studies of Broccoli, Turnip Seed, and Hemp Crops

Kristine R. Buckland[1], Taylor A. Bates[2], Alec Dyer[1], Ann Rasmussen[1], Lloyd L. Nackley[1], and Cynthia M. Ocamb[2]

KEYWORDS. **Alternaria, black leg, disease, gray mold, unoccupied aerial system**

ABSTRACT. **Disease detection through traditional techniques such as scouting fields on foot, molecular assays, or morphological identification of plant pathogens is time-consuming and costly. Scouting for disease in the field can be extremely subjective and largely depends on the scout's experience and knowledge of pathogen identification. Unoccupied aerial systems-based remote sensing on specialty crops has the potential to save labor, enable earlier detection of plant biotic stress and abiotic stress, and allow easier access to fields during wet conditions. For simple measurements, such as canopy cover, remote sensing works well; however, more sophisticated measurements of plant health involve complex data processing and may be challenging to implement. The difficulty is compounded for plant–pest pairs that have no published literature about remote sensing to reference. Technological improvements are steadily advancing, but these advances have led to short-term obsolescence, which remains an obstacle in the development of remote-sensing programs. Case studies of the following three different fungal diseases important in western Oregon crop production are presented: Alternaria black spot on broccoli, black leg on turnip, and gray mold on hemp. Remote sensing technologies present an objective approach to sampling that can address many concerns associated with traditional field sampling. These techniques can serve as a viable alternative that facilitate the development of more insightful integrated pest management programs that are essential for future agricultural efficiency.**

Unoccupied aerial systems (UAS), commonly known as drones, are increasingly important crop management tools. Drones can potentially serve in many different roles in food crop production systems, including spraying pesticides, dispersing beneficial insects, and plant health monitoring (Buckland et al. 2020; Merz et al. 2022; Pathak et al. 2020). Currently, in western Oregon, most drone operations are conducted by third-party companies contracted by growers because of equipment cost and the immense input of time and training to optimize drone systems. As drone systems and analysis software continue to evolve, there are increasing opportunities to adopt this technology; however, barriers remain.

Among the most technically difficult jobs accomplished with drones in agriculture is remote sensing for plant health monitoring. Remote plant health monitoring has the potential to save labor costs compared with traditional field scouting and offers the potential of early detection of both biotic and abiotic plant problems. While large-acreage crops such as corn and soybean have well-developed models implemented in user-friendly software packages, specialty crops require significant additional research to benefit from this technology.

Oregon is rich in specialty crop production. Top horticultural commodities include nursery crops, vegetables, and specialty seeds (US Department of Agriculture–National Agricultural Statistics Service 2023). Specialty crop fields in Oregon are generally smaller and more highly diverse than larger horticultural production regions. Because of the number of different crops grown as well as the high cost of equipment, software, and specialized labor, remote plant health scouting programs on farms are uncommon in Oregon. Yet, remote sensing programs for plant health have the potential to offer early intervention opportunities.

The difficulty of using UAS for disease detection varies greatly with the visibility of disease symptoms and signs and the ability of the drone camera to capture an image with the needed resolution or orientation. Most of the literature emphasizes the utilization of multispectral or hyperspectral digital images for disease detection (Barbedo 2013); however, in the infancy of disease detection by remote sensing, red-green-blue (RGB) was the most commonly used method and still has value because of its low cost and ease of use. Many studies have reported success using RGB images for disease detection (Arivazhagan et al. 2013; Barbedo et al. 2016; Camargo and Smith 2009a, 2009b; Neumann et al. 2014). Reviews by Barbedo (2013, 2016) have provided practical explanations for why RGB is still relevant for disease detection. Despite the ability of RGB to detect plant diseases, studies that have compared RGB and multispectral images have often reported that multispectral cameras are more proficient for disease detection (Abdulridha et al. 2019; Dammer et al. 2011). Many of these findings are likely attributable to the reflectance of vegetation in the near-infrared region of the electromagnetic spectrum often captured in multispectral data, but not in RGB data.

Spectral indices and vegetation indices have become primary approaches for disease detection by multispectral users (Behmann et al. 2014; Candiago et al. 2015; Naidu et al. 2009; Yang et al. 2007). A vegetation index is a spectral calculation between bands meant to reveal characteristics of the plant that are not apparent otherwise. Many vegetation indices have been developed over the past few decades, including spectral indices designed for a single disease (Mahlein et al. 2013). Currently, specific indices are not yet as effective as a well-trained field scout for disease detection. Instead, the indices detect the result of disease, such as poor canopy cover or chlorotic leaf tissue.

Machine learning, a field of artificial intelligence, focuses on computer

Received for publication 10 Jan 2025. Accepted for publication 4 Apr 2025.

Published online 13 Jun 2025.

[1]North Willamette Research and Extension Center, Oregon State University, Aurora, OR 97002, USA

[2]Department of Botany and Plant Pathology, Oregon State University, Corvallis, OR 97331, USA

K.R.B. is the corresponding author. E-mail: kristine.buckland@oregonstate.edu.

https://doi.org/10.21273/HORTTECH05599-25

algorithms that can learn from data and improve their accuracy over time through experience. When applied to plant disease detection using remote sensing, the process involves five steps: data acquisition, data processing, model training, model testing, and application. This work used a support vector machine that comprised supervised max-margin models with associated learning algorithms that analyzed data for classification and regression analysis. Support vector machines have been well-studied and frequently used in agriculture disease detection models (Rumpf et al. 2010).

In addition to the variability of equipment capabilities, disease expression in different crop species and cultivars can vary widely. Because of the differences in crop plant color and reflectance, a model that detects powdery mildew on one plant species may not perform well on another crop, even if symptoms of disease appear similar to human scouts. Collecting both UAS imagery and proximal data to "ground-truth" when beginning to use a UAS for plant health is important to understanding what the images and vegetation indices are actually conveying. Remote sensing of the UAS is not currently a substitute for an on-the-ground scouting program. This series of cases studies reported here aimed to evaluate the potential for disease detection efforts via UAS for specialty crop fields in western Oregon. In each study presented, our hypothesis was that disease detection would be similar with the use of drone-acquired images and visual ratings. Details of data collection and data processing are provided in the Supplemental Material. Please review these details before reading each case study.

Case studies: Three disease detection trials of specialty crops

Broccoli–Alternaria black spot

The first project we conducted with UAS involved collecting multispectral imagery of a field trial at the North Willamette Research and Extension Center (see Supplemental Fig. 1 for map) and evaluating the effets of two fungicide treatments, chlorothalonil and fluazinam, with a nontreated control on an Alternaria foliar disease (black spot) in broccoli as part of a product efficacy trial. Broccoli (*Brassica oleracea*) is afflicted by Alternaria diseases (Black Spot, Gray Leaf Spot, Pod Spot). *Alternaria brassicae* and *Alternaria brassicicola* can infect leaves, petioles, stems, flower parts, and seed pods of a wide range of Brassicaceae crops and weeds. These fungi survive on residues of infected crucifer crops and weeds, producing asexual spores (conidia) when conditions are conducive and the debris is on the soil surface. Older leaves and older plants are more susceptible to Alternaria black spot. Small, dark or yellow leaf spots first develop and enlarge to circular areas that are brown to gray in color with or without concentric rings and possibly with black or purple borders and/or surrounded by yellow halos. Sometimes the leaf spots are limited by leaf veins, so the spots are angular in appearance rather than circular. Visual rating methods are detailed in S2 of the Supplemental Material.

A Micasense RedEdge–M (AgEagle Aerial Systems Inc., Seattle, WA, USA) optical sensor containing five multispectral bands was fixed to the DJI Matrice 210 RTK (SZ DJI Technology Co. Ltd., Shenzhen, China) UAS platform. Camera and platform specifications are detailed in S3 of the Supplemental Material. The UAV was flown at 10 m and 20 m above ground level on a plot measuring 4046 m^2 between 11:00 AM and 1:00 PM. Flights contained 80% image overlap and a double grid flight pattern using the DJI Pilot software (SZ DJI Technology Co. Ltd., Shenzhen, China). A reflectance panel was imaged before and after flights for radiometric calibration. Then, with the true reflectance values of the panel for each wavelength captured by the camera given by Micasense, radiometric calibration was completed in Pix4Dmapper to convert the digital numbers captured by the image to true image reflectance (Pix4Dmapper Pro version 4.2.27). Images were stitched together in Pix4D mapper and exported to ArcGIS, where plots were identified as separate areas of interest and subjected to analysis.

We detected significant differences among treatments across three indices: normalized difference vegetation index (NDVI) (Brecht 2018; Pettorelli 2013); normalized difference red edge (NDRE) (Fitzgerald et al. 2010) and near-infrared reflectance (NIR); and optimized soil adjusted vegetation index (OSAVI) (Brecht 2018) (Fig. 1). The chlorothalonil-treated plants consistently showed the highest reflectance. The index maps present the reflectance values for each respective index in a color ramp display (Fig. 2). All index maps with NDRE, NIR, and OSAVI showed similar results of vegetation health within the treatment regions. Treatment 2 had higher values for the indices shown in red, which is an indication of canopy coverage. The canopy coverage for treatment 2 is the largest, and treatment 3 shows the lowest canopy coverage.

However, on-the-ground visual ratings (Ocamb et al. 2019) showed that the story was more complicated than fungicide efficacy measurement. While plants in fluazinam-treated plots had a significantly lower disease incidence than that of chlorothalonil-treated plants, it also caused phytotoxicity in the broccoli that was observed as a faint foliar chlorosis. The UAS reflectance data indicated changes in canopy coloration as a result of phytotoxic effects, but not the presence of dark-colored leaf spots. Alternaria black spot was relatively less visible in remote overhead images than phytotoxicity; therefore, phytotoxicity and possibly reduced canopy cover resulted in the difference in the UAS imagery analysis. This simple case study shows the importance of collecting traditional proximally sensed disease ratings for crops, at least initially, to ensure that the measurements taken using UAS actually convey the disease incidence/severity rather than other biotic or abiotic stressors.

Turnip–Black leg

A machine learning model was developed to detect black leg in turnip seed fields (Bates 2021). Black leg is a fungal disease incited by *Plenodomus lingam* (syn. *Leptosphaeria maculans*, anamorph: *Phoma lingam*) and *Plenodomus biglobosus* (syn. *Leptosphaeria biglobosa*) that is problematic for crucifer vegetable crop producers and seed growers, including winter canola producers, where overwintering of crops is required for vernalization and subsequent seed production (Fig. 3). Outbreaks of black leg in conventional specialty seed production in western Oregon had been absent since the

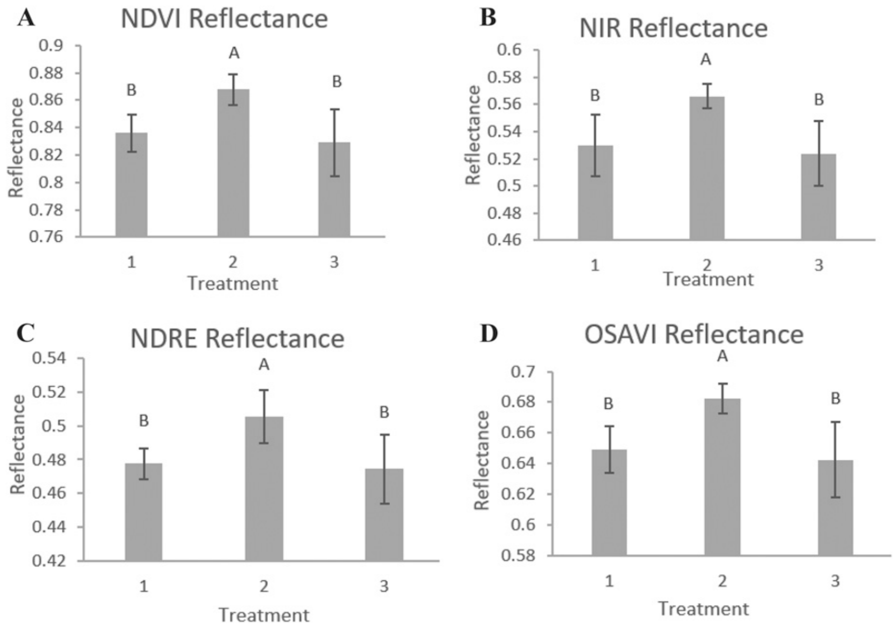

Fig. 1. Mean reflectance values (n = 4) for treatments with standard deviation are reported for normalized difference vegetation index (NDVI) (A), near-infrared (NIR) (B), normalized difference red edge (NDRE) (C), and optimized soil adjusted vegetation index (OSAVI) (D). Means not sharing a letter are significantly different using the Tukey-Kramer adjustment for multiple means comparisons at a level of significance of $P = 0.05$. Treatment 1 = nontreated control; treatment 2 = chlorothalonil applied weekly; treatment 3 = fluazinam applied weekly.

1970s; however, widespread disease was detected in 2014 (Claassen et al. 2021).

The environmental conditions are unique in western Oregon, making this area among the few regions in the world where climatic conditions allow for the production of quality Brassicaceae seed. However, the cool, wet conditions during late fall through early spring months in western Oregon create an ideal environment for black leg outbreaks, which can reduce yield of Brassicaceae plants through plant stunting and death as well as affecting seed quality. Seed harvests fail the required seed certification testing process if the black leg fungus is detected in seed testing, which renders the seed lot worthless. The wet conditions cause monitoring of black leg to be problematic, while spring scouting is also hampered by inflorescences taking over the space between plant rows.

Turnip sites. Turnip leaves affected by black leg were collected on 7 and 15 Mar 2019 from seed fields at two commercial farms in the Willamette Valley in western Oregon. Unmanned aerial vehicle (UAV) flights were also conducted at these fields on the same dates and selected based on cloud-free days during the winter months when leaf spot could be observed. Symptomatic leaves were collected to supply sufficient plant material representative of healthy tissue and diseased portions. *Plenodomus* leaf spots in selected turnip seed fields were not identified to species with molecular testing, but they were documented with images and determined to be *Plenodomus*-induced leaf spots based on characteristic symptoms and signs, including the production of pycnidia and purplish to pinkish cirrhus (conidia) that are characteristic of *Plenodomus lingam* and *Plenodomus biglobosus* from a subset of pycnidia. Following UAV flights and the collection of more than 100 diseased leaves from each location, leaves were placed in a moist chamber and returned to the laboratory. Diseased leaf specimens were either placed in a cold room (≈5 °C) for preservation for a maximum of 48 h or immediately used for image collection. Visual disease rating methods are detailed in S2 of the Supplemental Material.

Turnip data acquisition. An optical sensor capturing five multispectral bands (Micasense RedEdge–M; AgEagle Aerial Systems Inc.) was fixed to the DJI Matrice 210 RTK (SZ DJI Technology Co. Ltd., Shenzhen, China) UAV platform. The UAV was flown at 10 m and 20 m above ground level on a 4046-m^2 plot between 11:00 AM and 1:00 PM. Flights contained 80% image overlap and a double grid flight pattern using the DJI Pilot software (SZ DJI Technology Co. Ltd., Shenzhen, China). A reflectance panel was imaged before and after flights for radiometric calibration.

The optical sensor was also mounted to a PVC structure approximately 1.5 m above ground level with a power cable running to a laptop serving as the power source. The optical sensor was directed downward where the sensor view area included a black tarp and plastic tray as the background with a single turnip leaf placed at the center. Beside the tray was a reflectance panel used for radiometric calibration. Turnip leaves with leaf spots characteristic of black leg were imaged outdoors under the PVC structure between 11:00 AM and 1:00 PM to ensure properly lit photos. Images of 60 to 100 turnip leaves were collected for each of the two field locations on both dates with a spatial resolution of approximately 0.1 cm and 12-bit radiometric resolution. Details of data processing are provided in S4 of the Supplemental Material.

Classification and assessment of black leg on turnip. A clear division was observed between the "*Plenodomus*-affected" (diseased) and "healthy plant tissue" (nondiseased) pixels (Fig. 4). A total of 34 support vectors were used to determine a hyperplane for the binary classification of pixels when applying the support vector machine (SVM) model with a Gamma = 0.1 and cost = 1.

Of the 676 total pixels tested in the model, 96.8% were accurately classified as either diseased or nondiseased, while 3.2% were misidentified as either false-positives or false-negatives (0.04 and 0.03, respectively). The model had specificity of 0.96 and sensitivity of 0.97.

The final assessment of the SVM binary classifier was confirmed with classification of four individual leaves containing 15,519 pixels (Fig. 5). Classification of pixels in the four leaves resulted in an average accuracy of 97.0% and Kappa coefficient

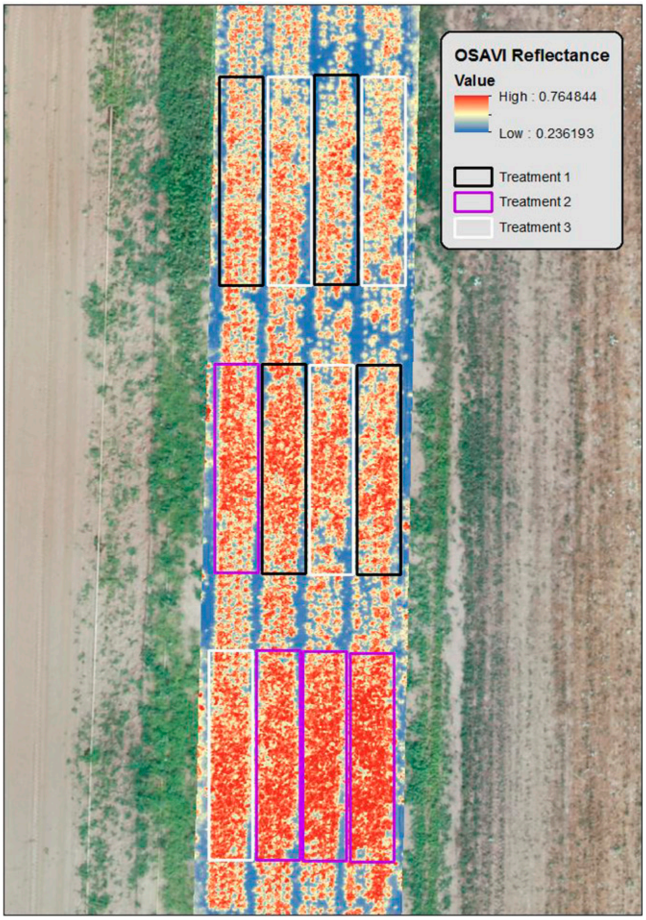

Fig. 2. Optimized soil adjusted vegetation index (OSAVI) images were collected at an experimental broccoli planting using the Micasense RedEdge-M Sensor.

of 0.60. The specificity was 0.99 and sensitivity was 0.48.

Hemp–Gray mold (botrytis bud blight and stem canker)

Botrytis spp. can thrive under a range of environmental conditions, but environmental conditions along with several biological and agricultural factors will influence the development of disease. The two most important environmental factors for the germination of a *Botrytis* conidium are relative humidity and ambient temperature. While this pathogen is known for its extremely high genotypic and phenotypic plasticity, which give it the ability to adapt to many environments and allow *Botrytis* spp. to persist within a broader spectrum of temperatures and humidity ranges, the optimal conditions are temperatures between 15 and 20 °C with the presence of free water or relative humidity above 93% (Carisse 2016). Generally, the minimum period of time during which the temperature and relative humidity requirements should be met is 4 h, but the longer the conducive environmental conditions persist, the greater the likelihood of an infection event, regardless of crop (Broome et al. 1995; Bulger et al. 1987). Cool to moderate temperatures and high relative humidity are common conditions in the Willamette Valley of Oregon, particularly in the late summer and early fall; these are high-risk factors for disease development caused by *Botrytis* in hemp plants. *Botrytis* is known to remain latent within the plant until the required environmental conditions are met in the infected host tissues. Once environmental conditions are favorable, it is only a matter of days before symptoms become visible; soon thereafter, disease can reach epidemic proportions if effective disease management strategies are not instituted (McPartland 1996).

Hemp floral organs serve as the primary infection court for *Botrytis* spp., but this fungus can also infect wounded tissues as well as senescing portions of a plant, and oftentimes it will remain quiescent before symptoms develop. While the primary mode for *Botrytis* infection of hemp is not well-studied, penetration is known to occur on other crop hosts through natural openings such as carpels (De Kock and Holz 1992) and stomata (Fourie and Holz 1995; Hsieh et al. 2001), although *Botrytis* may infect through an undamaged cuticle in some cases (Nelson 1951). Symptoms on hemp flowers begin with fan leaflets turning yellow and wilting, followed by browning of the pistils. Soon after, flowers become covered in gray mycelium, conidiophores, and conidia, resulting in a gray to brown and fuzzy appearance that gives rise to the disease called gray mold (McPartland 1996). Soon after, disease can spread encompassing large portions to entire inflorescence (Fig. 6). Although gray mold on hemp flowers is a primary focus of this research project, *Botrytis* spp. can cause damping-off of seedlings or incite stem cankers when plants are nearing full maturity, especially on cultivars grown for fiber production (McPartland 1996; McPartland et al. 2000).

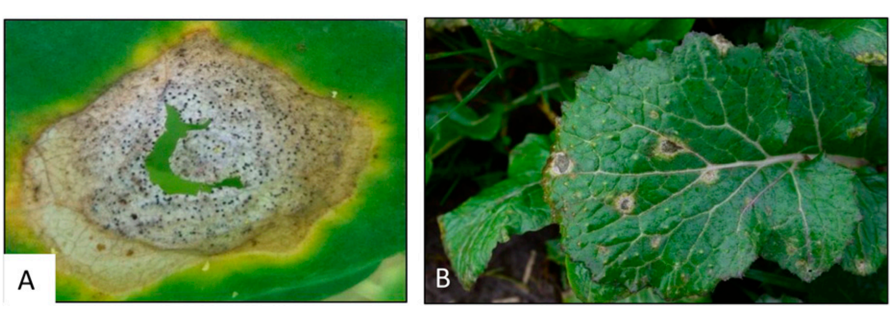

Fig. 3. Leaf spot on turnip leaf showing pycnidia formation and shothole effect in the center of leaf lesions typical of Phoma leaf spot caused by *Plenodomus maculans* and/or *P. biglobosa* in western Oregon (A). Turnip leaf displaying symptoms of leaf spots characteristic of black leg (B) (Image A provided by C. M. Ocamb).

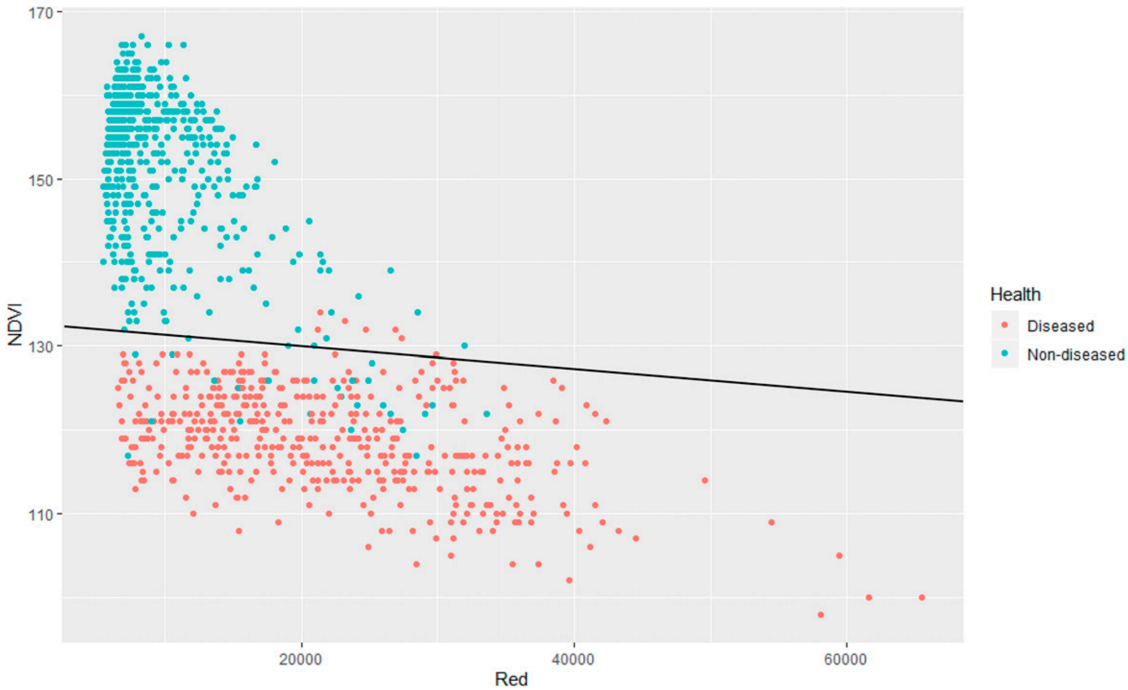

Fig. 4. A plot of pixels used in the training data set to determine the hyperplane of the support vector machine (SVM) model with a hyperplane drawn through the training data using 34 data points as support vectors. When testing data are used, points below the line are classified as diseased, while pixels above are classified as nondiseased.

Hemp site. On 18 Jun 2020, 0.28 ha (2833 m^2) of the hemp cultivar 'White CBG' were planted at the Oregon State University Botany Field Laboratory in Corvallis, OR, USA, for a biofungicide efficacy trial of gray mold on hemp. Pregerminated seeds were hand-sown in a randomized complete block design with five replicates.

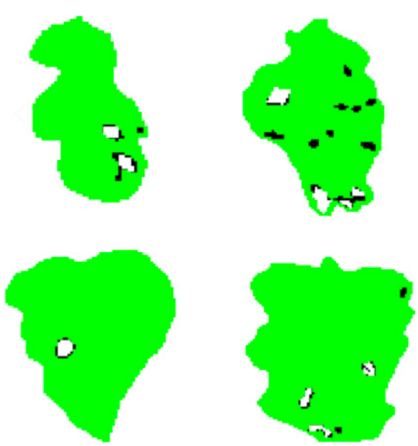

Fig. 5. Four turnip leaves removed from the background with pixels classified as either nondiseased (green) or diseased (white). The black pixels indicate pixels that were manually selected as diseased and true positives that were misclassified by the support vector machine (SVM) model.

Each plot had two rows of 10 plants, with plants spaced at 1.8 m between rows and 1.2 m within rows. There were two plants between replicate blocks and three plants between plots within a replicate block providing a 3.66-m buffer. Additional details of this study can be found in Bates (2021). Visual disease rating methods are detailed in S2 of the Supplemental Material.

Hemp data acquisition. *Visual survey of the field.* From June to October, plants were surveyed for gray mold; *Botrytis* was first observed causing disease within the hemp field on 22 Sep 2020. *Podosphaera macularis* and *Fusarium* spp. were also noted on some plants. Visual assessments of gray mold incidence in the uppermost 30-cm portion of eight individual inflorescence on each of five randomly chosen plants in each plot were conducted on 25 Sep, 2 Oct, and 9 Oct 2020. Incidence data were analyzed as repeated measures in a generalized linear mixed model assuming a binomial distribution of the response variable. Treatment, rating date, and their interaction were fixed effects. Replicate block was a random effect. Temporal correlation of residuals was modeled assuming a first-order autoregressive covariance structure. Analyses were conducted using the GLIMMIX procedure in SAS version 9.4 (SAS Institute, Cary, NC, USA).

Aerial survey of the field. The UAV flights were conducted on 26 Aug, 22 Sep, and 7 Oct 2020, between 11:00 AM and 1:00 PM for each flight. The UAV was flown at 10 m above ground level and ranged from 21 to 24 min, with 80% image overlap and a double grid flight pattern covering 3642 m^2 using DJI Pilot software. A reflectance panel was imaged before and after flights for radiometric calibration. The aircraft platform was the DJI Matrice 210 RTK (Supplemental Table 1) with a Micasense RedEdge–M (Supplemental Table 2) optical sensor containing five multispectral bands. Spatial resolution was 0.69 cm, with a 12-bit radiometric resolution. Details of data processing are provided in S4 of the Supplemental Material.

Classification and assessment of gray mold on hemp. A generally high rate of "unhealthy leaf" pixel misidentification by all models tested led to the development of a novel vegetation index, Green Red Modified Vegetation Index (GRMVI). Initially, differences in the four training classes for each spectral band and vegetation

Fig. 6. Hemp inflorescence with a single flower infected with *Botrytis*, the causal agent of gray mold (A). Gray mold along an inflorescence after disease spread among flowers resulting in flower necrosis (B).

index were assessed for relatedness in pixel ranges and overlap with an emphasis on the minimum and maximum values. Means of classes were less significant than large overlaps in range regarding SVM and RF classification models. Box and whisker plots of the GRMVI with outliers included (Fig. 7) or removed (Fig. 8) are provided and were used for the hemp–gray mold model development. With the outliers included, the maximum value for "*Botrytis*-infected inflorescence" (unhealthy bud) was 0.91 and the minimum for "unhealthy leaves" was 0.38, resulting in a difference of 0.53 in digital number values. With outliers removed, the maximum value for "*Botrytis*-infected inflorescence" (unhealthy bud) was 0.64 and the minimum value for "unhealthy leaves" was 0.54, resulting in a difference of 0.10 in digital number values. By merging "healthy inflorescence," "unhealthy leaf," and "healthy leaf," no differences in minimums and maximums are seen because "unhealthy leaves" represent the lowest values in the merging of these three classes. Because SVM models use support vectors to generate a hyperplane, understanding the range of data is more useful than comparing means. Box and whisker plots provide a clear visual depiction of the data spread along with the outliers, which tend to define the model's hyperplane, particularly for an SVM. In many pixel-based analyses using machine learning, outliers are not removed from the training classes; however, this approach of removing outliers has seen acceptance in other fields because of increased model accuracy (Maniruzzaman et al. 2018). Outliers were removed from this model for two reasons. First, when generating a training data set, a limited number of misclassified pixels is not unexpected. If the data set is extremely large, then these misclassified pixels have less of an impact on the generated hyperplane. Second, machine learning model building should use a cyclic process of model creation, repeated testing, and fine-tuning of the model until the best results are found. Through this repetition of model creation and testing, the removal of outliers provided a hemp–gray mold model with the best results with the data used as indicated in the confusion matrix. Pixels designated as outliers in the hemp model were primarily pixels displaying very low levels or early stages of disease, or they were chlorotic or necrotic leaves that visually appeared as gray mold-affected inflorescence through the values of the GRMVI data.

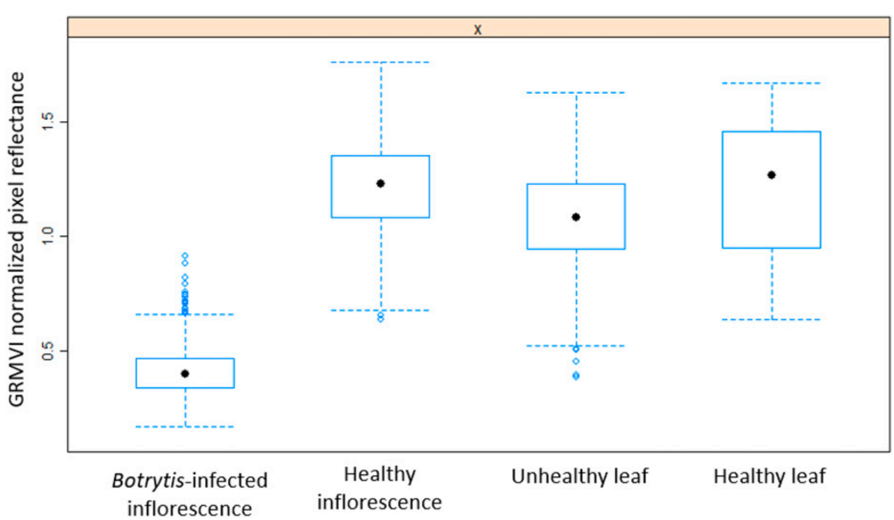

Fig. 7. The box and whisker plot of gray mold on hemp training data of Green Red Modified Vegetation Index (GRMVI) pixels with outliers included in the four training classes.

The set of bands and vegetation indices were additionally tested for differences by an analysis of variance (ANOVA) when examining data with four classes; then, they were further assessed with a pairwise t test of means adjusted by Bonferroni. This analysis helped to remove vegetation indices or bands where there were no significant differences in observed means and would not have contributed significantly to the model's ability to classify training groups. With two classes, an ANOVA was conducted using GRMVI, and a significant difference was seen between classes ($P < 0.01$). Mean Decrease Gini was used as a final assessment to determine variable importance and what should be used for the hemp–gray mold model. Bands or

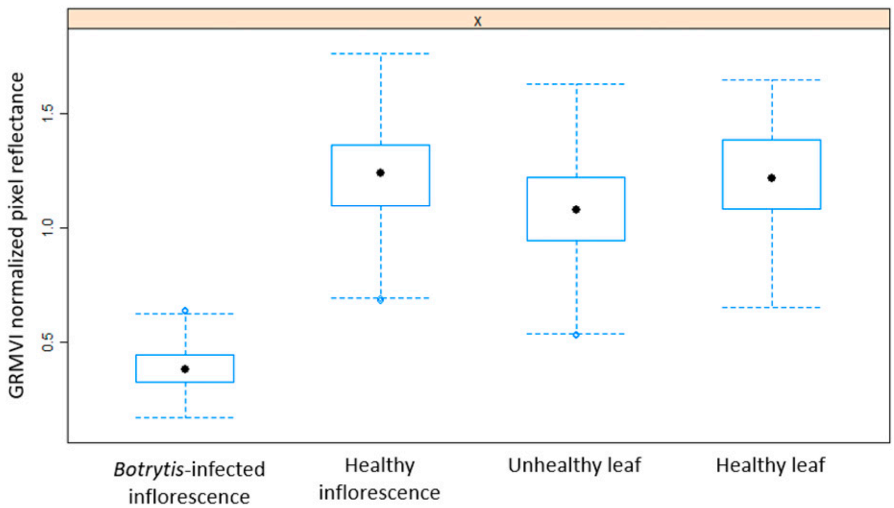

Fig. 8. The box and whisker plot of gray mold on hemp training data of Green Red Modified Vegetation Index (GRMVI) pixels with outliers removed from the four training classes.

vegetation indices with greater Mean Decrease Gini values are associated with contributing to a better model fit. Table 1 lists the significance given to each variable for both classes, "*Botrytis*-infected inflorescence" and "other plant tissue," in addition to the four classes of "*Botrytis*-infected inflorescence," "healthy flowers," "unhealthy leaves," and "healthy leaves." The GRMVI was the most important model for the two classes and was, subsequently, the sole variable selected for the final gray mold–hemp model.

The final gray mold–hemp model used an SVM of Gamma = 1 and cost = 1 with the new vegetation index, GRMVI, which was determined to provide the greatest balance of accuracy with the fewest variables included. The SVM model used 91 support vectors (2340 classified testing pixels) and resulted in an accuracy of 99.15% and Kappa value of 0.97, with sensitivity of 0.97 and specificity of 0.99.

Table 1. Mean Decrease Gini values associated with each band or vegetation index when assessing variables with two training classes and four training classes.

Band or vegetation index	Mean decrease Gini (two classes)	Mean decrease Gini (four classes)
SAVI	76	478
OSAVI	85	490
RECI	6	31
GCI	32	237
MSRE	7	37
MSR	87	507
GNDVI	25	271
NDRE	7	40
NDVI	86	438
GRVI	336	260
TGI	257	384
GRMVI[i]	430	315
Red edge	30	47
Red	7	167
Near-infrared	37	50
Green	48	178
Blue	8	35

[i] Green Red Modified Vegetation Index (GRMVI) was the selected variable for the gray mold-hemp support vector machine model.

GCI = Green Chlorophyll Index; GNDVI = Green Normalized Difference Vegetation Index; MSR = Modified Simple Ratio; MSRE = Modified Simple Ratio Red-Edge; NDRE = Normalized Difference Red Edge; NDVI = Normalized Difference Vegetation Index; OSAVI = Optimized Soil Adjusted Vegetation Index; RECI = Red-Edge Chlorophyll Index; SAVI = Soil Adjusted Vegetation Index; TGI = Triangular Greenness Index.

Field validation of the SVM model indicated misclassification of "unhealthy leaves" as "*Botrytis*-infected inflorescence." Extraction of the hemp plants from the background noise, such as brown soil and weedy vegetation, was one of the greater challenges of this portion of the remote sensing work with hemp, but it can be accomplished through various means (Hamuda et al. 2016). Because of many false-positive results of "unhealthy leaves," another step was added to the analysis to reduce pixels falsely identified as "*Botrytis*-infected inflorescence" to "other plant tissue." To conduct extraction of the hemp plants from the field site used in our study, conservative methods of removing the outer edge of most plants were applied to ensure that little to none of the soil appeared in the analysis because soil generally causes a false-positive result. This post-SVM step used Triangular Greenness Index (TGI) to help optimize the accurate designation of pixel classification, creating an iterative process. The differences between classes of pixels in the TGI, with and without outliers, are shown in Figs. 9 and 10, respectively. With the outliers included, the maximum value for "*Botrytis*-infected inflorescence" was −680 and the minimum for "unhealthy leaves" was −13,855, resulting in a difference of more than 13,000 in digital number values. With outliers removed, the maximum value for "*Botrytis*-infected inflorescence" was −680 and the minimum value for "unhealthy leaves" was −3065, resulting in a difference of 2385 in digital number values. A threshold of −3000 effectively corrected for false-positive results of "unhealthy leaves" and was included in the analysis, which changed "*Botrytis*-infected inflorescence" with a digital number greater than −3000 to "other plant tissue." An example of the intersection between canopy height model, segmented NDVI, and 8-pixel buffer is illustrated in Fig. 11. Each SVM-classified plot with the TGI threshold as well as individual plants are shown in Fig. 12.

The sampling of hemp inflorescence pixels from the classified model derived from the SVM model and

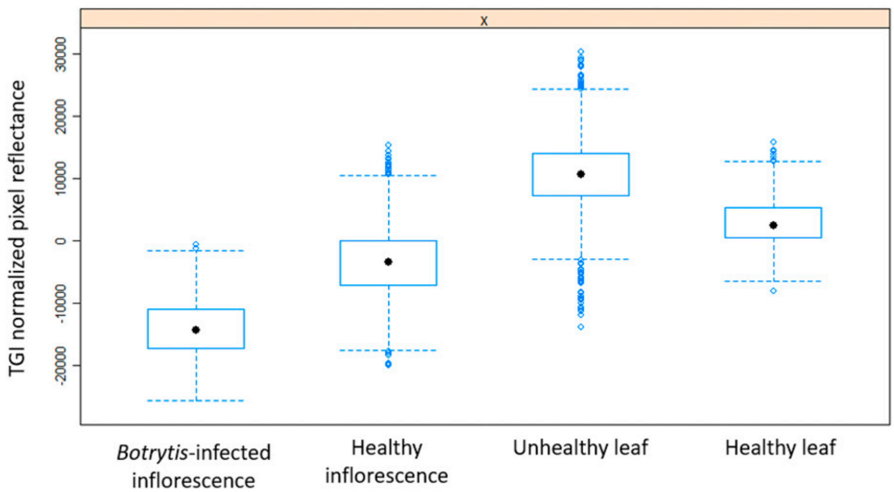

Fig. 9. The box and whisker plot of gray mold on hemp training data of Triangular Greenness Index (TGI) pixels with outliers included in the four training classes.

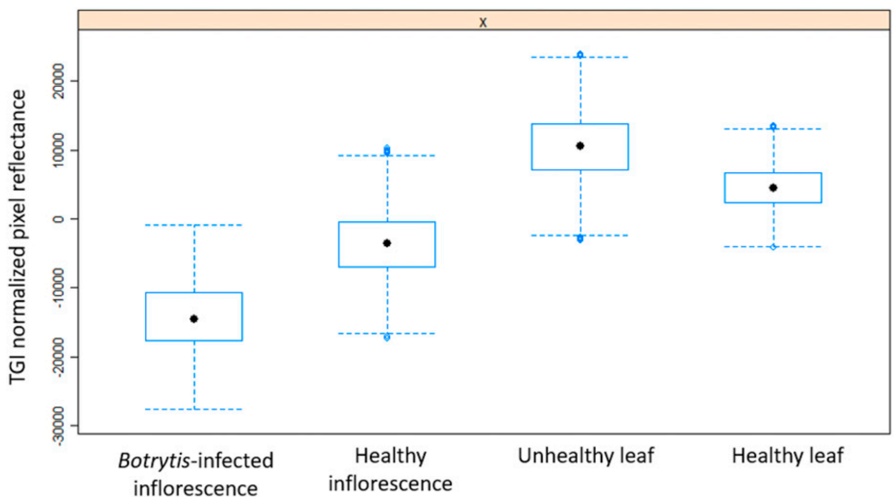

Fig. 10. The box and whisker plot of gray mold on hemp training data of Triangular Greenness Index (TGI) pixels with outliers removed from the four training classes.

TGI threshold had 95.8% accuracy, with a Kappa of 0.80. The specificity was 0.99 and the sensitivity was 0.70.

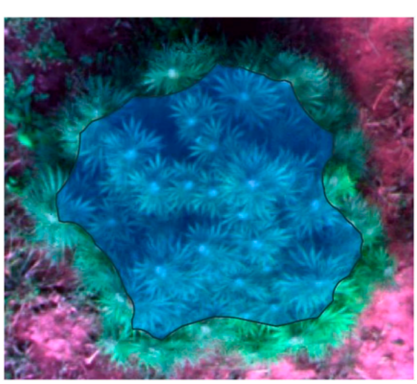

Fig. 11. Hemp plant with a blue polygon indicating the region being extracted through the overlap of the ArcGIS Pro segmentation function, canopy height model, and 8-pixel buffer.

The ANOVA indicated significant treatment effects assessed using field-based disease incidence (the conventional on-foot disease assessments) ($P \leq 0.0001$), classified model rating disease incidence ($P = 0.0885$), and reference false color images disease rating incidence ($P = 0.0289$). Inflorescence in the nontreated control had the greatest estimated percentage of gray mold using each assessment method (Table 2). However, the mean percentage of the gray mold incidence for all treatments was much larger with field-based ratings than that with either the classified model or the reference false color images disease rating method. The mean incidence percentage of gray mold rankings of the classified model and that of the reference false color images disease assessments were the same. Significant differences between nontreated control and the three fungicide treatments were observed in both field-based incidence and reference false color images incidence ($P \leq 0.05$). The rank order of mean incidence of the field-based rating method and that of the classified model method differed between plants in plots that received treatments 1 and 2, but the means were not significantly different with either treatment.

Field-based incidence ratings, classified model incidence ratings, and reference false color images incidence ratings were plotted for each treatment at each block. Incidence ratings from the classified model ratings had a low R^2 of 0.26 when regressed against disease incidence using field-based assessments (Fig. 13). Incidence ratings from the reference false color images and field-based disease assessments also had a low R^2 value of 0.32. Disease assessment ratings from the classified model ratings had the highest R^2 correlation with reference false color images disease ratings of 0.85.

Discussion

Alternaria on broccoli

The results of this research illustrate the complexity of developing models for disease detection using remote sensing under various field conditions. While the broccoli field trial identified a difference in plant growth between treatments, visual ratings were needed to identify abiotic stress from pesticide applications, as opposed to disease damage. However, both black leg on turnip and gray mold on hemp were successfully identified through remote sensing with a multispectral sensor and machine learning techniques after more advanced data processing approaches and, in the case of black leg, increased resolution achieved with a stationary frame inside the greenhouse.

Black leg on turnip

The black leg–turnip model did not use outlier removal; instead, it adhered to a more conventional machine learning model development method set. In the turnip training data set, overlap occurred, with "nondiseased" pixels merging into the "diseased" cluster of pixels. This same problem arose in the training data set for "*Botrytis*-infected inflorescence" and "other plant

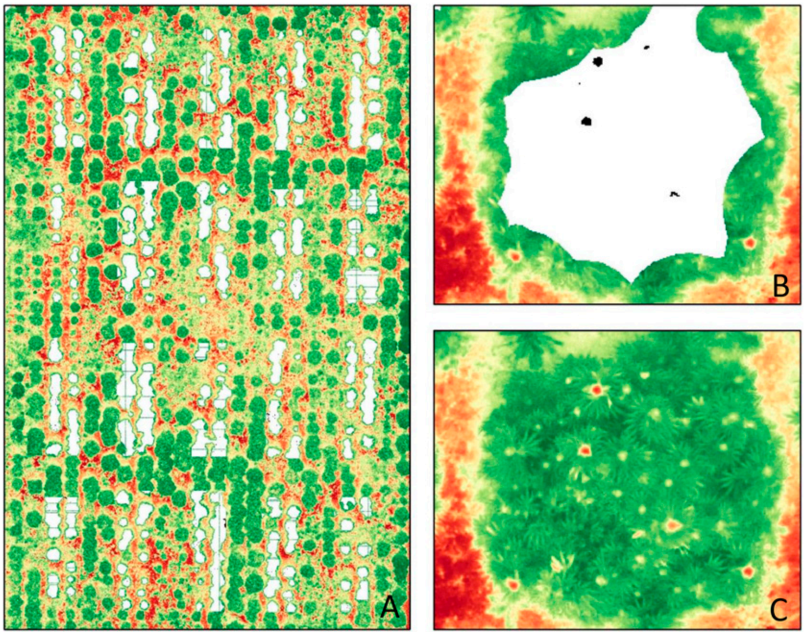

Fig. 12. A normalized difference vegetation index (NDVI) false color image of a hemp field at the Oregon State University Botany and Plant Pathology Field Laboratory with extracted plant polygons in white for each treatment plot (A). An individual plant with white pixels identifying healthy plant tissue and black identifying *Botrytis*-infected inflorescence (B). The hemp plant from (B) without identified pixels as an NDVI false color image with red pixels indicating disease within the plant (C).

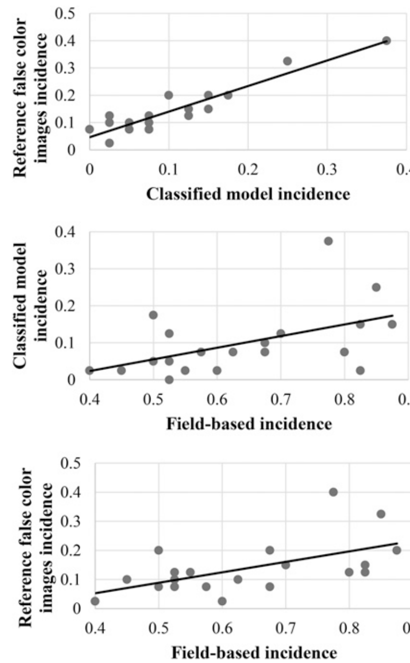

Fig. 13. Gray mold incidence for four treatments with five replicates by two disease assessment methods and a third disease assessment using by-hand classification of false color images. The conventional field-based and classified model with a support vector machine (SVM) and Triangular Greenness Index (TGI) threshold regression (R^2 = 0.26) (A). The field-based and reference false color images disease incidence regression (R^2 = 0.32) (B). The classified model and reference false color images disease incidence regression (R^2 = 0.85) (C).

tissue." This could be a result of genuine overlapping of reflective values of the diseased and nondiseased classes, an imperfect training data set, outliers, or an insufficient number of training values used in the model.

The results of the SVM models developed for black leg on turnip and gray mold on hemp appear to be sufficient for ex situ applications based on the model validation findings using the test data. However, with the described flight and camera parameters for the equipment in this study, the black leg turnip model was not successful in field conditions. With the use of a more capable multispectral camera, the model should be reevaluated for use at a field scale because image resolutions at the scale of the greenhouse study are now available at greater distances that could result in less leaf disturbance from UAS downdraft.

Gray mold on hemp

The development of a novel vegetation index, GRMVI, was necessary and revealed differences in reflectance values for hemp pixel classes not seen in the other bands or vegetation indices. However, this study indicated that high-accuracy pixel classification with few false-negative and false-positive results does not directly translate to dependable disease identification in field-based applications. Although the estimated disease incidence was much lower in the classified model compared with the field-based ratings, ranking of treatment means by both methods were similar. Although rankings were similar at the experimental level, a low correlation between disease incidence ratings were found for each treatment plot when comparing the two methods. Accuracy in this context is always in reference to a metric used to evaluate algorithms on binary and multiclass classification datasets. Accuracy is the percentage of instances that are correctly classified. High accuracy is a positive indicator of the model's ability to correctly determine diseased and nondiseased plant tissue via pixel classification.

The need to apply a buffer area to facilitate the extraction of hemp plant tissue from soil background pixels was problematic and demonstrated the need

Table 2. Gray mold incidence on hemp inflorescence for the field-based, classified model, and reference false color images-based disease assessment methods.

	Gray mold incidence (%)		
Treatment	Field-based[i]	SVM classified model[ii]	Reference false color images[ii]
Nontreated control	83.1 a[iii]	17.6 a	23.6 a
Treatment 1	59.1 b	6.6 ab	9.9 b
Treatment 2	58.0 b	7.5 ab	11.7 b
Treatment 3	55.5 b	5.4 b	9.5 b

[i] Field-based data rating (conventional on-foot assessment) was conducted on 9 Oct 2020.

[ii] Remote sensed data were collected on 7 Oct 2020 for both classified model and reference false color images disease assessment methods.

[iii] Means within the same column followed by the same letter are not significantly different based on a generalized linear mixed effects model and pairwise t test at $P \leq 0.05$.

for careful development of processes for remote disease detection specific to crop/pathogen combinations. Although not all pixels composing the plant were included in the final analysis, large enough regions of most plants were extracted for a representative sampling of the field. Unless the outer edges of the plants display more disease than the inner portion, which did not appear to be the case in this study, this conservative approach to plant canopy extraction seems acceptable as a work-around for the problems posed by exposed soil and other vegetation surrounding individual plants. However, the noise caused by soil and vegetation in this field that led to misclassification of pixels may be less of an issue in commercial hemp fields that use black plastic within the plant row, but plastic–culture adds complexity in field management, cost, and pest pressure. Because only the turnip leaves were manually extracted, rather than entire plants, false-negative and false-positive results were much less common, as would be expected. If whole turnip plants were extracted, then similar issues as posed by the hemp field would likely arise, making the classification process more difficult. Nonetheless, for any agricultural field-based application, extraction of the plants from the background is pertinent to obtaining accurate and meaningful analysis results.

To apply this technology under field conditions, a much lower level of false-negative results is necessary to make this remote sensing tool reliable. Through visual assessment of the classified pixels in the raster, it was clear that some of the false-positive results that appeared on the hemp image were attributable to necrotic and/or chlorotic foliage rather than *Botrytis*-infected inflorescence. This tends to be a reoccurring issue and is one of the greatest challenges of this work. It is an anticipated problem when using field data rather than greenhouse or laboratory-grown plants free of other abiotic and biotic factors that influence or mimic plant health and the appearance of yellowing or browning plant tissues.

The TGI showed the least amount of overlap between the classes "unhealthy leaves" and "*Botrytis*-infected inflorescence" among bands and vegetation indices examined. The maximum and minimums of both these classes, analyzed with and without outliers, were used to determine the threshold of −3000 to transfer pixels assigned to the "*Botrytis*-infected inflorescence" class to the "other plant tissue" class. This threshold resulted in fewer false-positive results. Although the inclusion of the threshold did slightly increase the occurrence of false-negative results, the impact of including the threshold was important enough for it to be part of the final model used for field testing.

When determining how the SVM model classified pixels, in some cases, one, two, or three pixels were correctly classified as "*Botrytis*-infected inflorescence," but they were not counted because four pixels was considered the minimum number necessary for classification as a "*Botrytis*-infected inflorescence." Lowering this threshold may have slightly influenced the results, but only to a small degree. The SVM model and TGI threshold resulted in high overall accuracy but low sensitivity, which is thought to be partly influenced by the TGI threshold among others. Many of the pixels changed by the threshold indicated either early signs or symptoms of the disease or contained a mix of diseased and nondiseased pixels. Therefore, this model did not have optimal classification capabilities needed to classify pixels that were in early stages of disease development or were a mosaic of diseased/healthy pixels. This was confirmed through visual assessment during classification, whereby slightly diseased inflorescences in false color images (NDVI and GRMVI) appeared faintly red, whereas very diseased inflorescences appeared deep red.

The final determination consisted of a comparison of the SVM and TGI pixel classification model (classified model) and conventional disease assessments (field-based) for measuring gray mold incidence on hemp. Among both sampling strategies, there was general agreement that the greatest disease incidence was observed in the nontreated control, and the lowest incidence was found in treatment 3; however, the middle two ranked treatments, treatments 1 and 2, had alternating rankings. Despite this switch, the means were not significantly different. The disease incidence estimates seen in the classified model were much lower percentages than those observed in the field-based disease assessments. This is likely attributable to the inability to detect disease symptoms or signs that are not visible from directly above the plant (nadir perspective); in other words, disease lower down the length of the inflorescence goes unseen when assessments are performed by an UAV. The classical field-based sampling assessed disease along the upper 30-cm length of the inflorescence, while the data used in the classified model most likely contained only the uppermost portions of each inflorescence and did not capture the sides or entirety of the 30-cm region because of the necessary buffer between plant tissue and soil surface included in the model. The nadir perspective of the aerial flights is one of the greatest challenges associated with remote disease detection via UAV for this reason.

Aerial remote sensing was also conducted 48 h later than the ground sampling disease incidence measurements. During this 48-h period, it may have been possible for disease incidence to increase and result in different levels of disease incidence for treatments 1 and 2 at the time of aerial sampling; however, the large differences in treatment means between these two methods made it seem highly unlikely that the time difference accounted for most of the treatment means disparity. Additionally, as previously observed, the classified model's sensitivity was too low to detect all signs or symptoms of Botrytis that were present. Disease observed through assessments using the reference false color images of the same inflorescences used in the classified model rating was slightly higher, but means generated by the reference false color images were still much lower than field-based disease assessments. Both the classified model assessment of disease incidence and the reference false color images incidence had the same ranking of treatments. This indicates that although the classified model may have low sensitivity, an increased sensitivity and associated decrease in false-negatives would not have changed the rankings of gray mold incidence seen among the fungicide treatments. While the rankings were the same among the reference false color images and the classified model, the reference false color images showed a significant difference between nontreated control and the three biofungicide treatments, while the classified model did not find a significant difference between nontreated and the three biofungicide treatments. This indicates that if the classified model had perfectly classified all hemp inflorescences, resulting in 100% overall accuracy and the equivalent to the reference false color images, then the significant differences observed among treatments would have been the same as those found in the field-based assessment method.

The comparison of disease incidence ratings for field-based assessments and the classified model resulted in a low R^2 value, which suggested large differences in incidence ratings between these two assessment strategies for each treatment plot. The R^2 value was slightly increased in the comparison of the reference false color images disease ratings with field-based disease incidence assessment; however, overall, both the classified model and the reference false color images ratings had a poor fit when compared with the field-based data. Mean disease incidence percentages for field-based rating in comparison with the other two methods showed large differences among treatments, but they also largely differed within each plot. Conversely, the reference false color images rating compared with the classified model rating for disease incidence resulted in a high R^2 value. This stronger relationship is not unexpected because both methods used the same aerial images captured by the drone. Both of these remote sensing disease assessment methods (reference false color images and the classified model) had less than ideal results when compared with those of the field-based assessment, reinforcing that hemp gray mold incidence data collected aerially via remote sensing failed to capture the proportional percentage of disease incidence that was detected by field-based disease assessment techniques.

Efficacy of disease detection methods

This research is the first report the detection of gray mold on hemp under field conditions; however, Ferentinos et al. (2019) detected gray mold on hemp in a greenhouse where other abiotic and biotic factors were present. This article is also the first to report the detection of black leg on a *Brassica* crop (Bates 2021). Others have identified leaf spot diseases on similar plants such as Cercospora leaf spot on sugar beet (Zhou et al. 2014) using a multispectral camera. Mahlein et al. (2010) detected Cercospora leaf spot on sugar beet using an SVM for data from a hyperspectral camera. This work contributes to the current literature by broadening our understanding of methods that can be used for remotely sensed disease detection. It also provides a novel vegetation index for disease detection (GRMVI) that may be of use for detecting disease in other host–pathogen systems. The detection of gray mold on hemp case study also presented an alternative technique to traditional methods of disease detection.

The remote sensing methods reported in this research were similar to what other researchers have reported in other pathosystems. The hemp–gray mold and turnip–black leg case studies used methodology similar to that outlined by Abdulridha et al. (2019); it consisted of image acquisition, preprocessing, image segmentation, feature extraction, and classification. These steps are generally the standard framework for many remote sensing and model building processes. Image acquisition in our research fell toward the lower end of flight/image acquisition elevation at 10 m above ground level for detection of gray mold in hemp and 1.5 m for black leg in turnip. Abdulridha et al. (2019) also collected images to detect laurel wilt in avocado at 10 m, but they were not collected via UAV. Similar to the turnip image acquisition case study, Dammer et al. (2011) acquired imagery at 2.4 m above wheat plants with *Fusarium* head blight; however, images have been taken as low as 25 cm from the plant (Bravo et al. 2003). Others have conducted flights at 120 m above ground level (Albetis et al. 2017) with limited success and at 40 m above ground successfully (Heim et al. 2019) based on overall accuracy assessments. Although there are many factors that require consideration because they ultimately dictate the flight parameters, increased imagery collection elevations that maintain accuracy should always be a goal.

The gray mold on hemp case study, along with many other studies that attempted to detect fungal diseases, incorporated fungicide applications that create varying degrees of disease incidence and severity (Franke and Menz 2007; Heim et al. 2019). This allowed for nontreated plots, which were heavily infected with disease, and treated plots that contained less disease, as well as the collection of ground truth data. We found this to be very helpful in our hemp gray mold study because it allowed for not only the presence of diseased plants and nondiseased plants at a plot level that could be used in statistical analysis but also provided the opportunity to compare remotely sensed results with ground truth disease incidence and application of this work in an agricultural setting. West et al. (2003) acknowledged the potential benefits of optical sensors for fungal disease detection in targeted spray treatments but mentioned the likelihood of underestimating the disease patch size, which was also found to be true in this study. Bravo et al. (2003) and Zhang et al. (2019) evaluated various plant cultivars with different levels of resistance to create disease gradients, which enabled a similar type of analysis and illustrated an additional application of remote sensing.

The case study set explored here demonstrated limitations to this research and subsequent application of this technology. Because the lesions caused by *Plenodomus* on leaves of turnip and other brassicas are relatively small, optical sensors we had access to did not have the spatial resolution required for the detection of black leg leaf spots on turnip for drone flights at 10 m and 20 m above ground level. Additional challenges arise when entire turnip plants are imaged ex situ rather than as individual leaves that are laid flat and imaged in situ. Field-like conditions, such as abiotic and biotic factors that influence the quality of image classification, will also increase the difficulty of remote sensing work. In gray mold on hemp, scaling up from a single acre to larger acreage may be difficult and would require increasingly longer flight times and data storage space, among other factors. Models developed from this thesis work should be considered preliminary and could be ineffective when used in another field or region, thus requiring additional training data on a field-by-field basis until a sufficiently large data set is developed for the respective models. Additionally, these remote sensing methods are limited to data collected from a nadir perspective and lack the optical ability to detect disease found lower in the canopy, inside the canopy, or along the sides of the plant and flowering/nonflowering stems.

The processes tested here need to be refined before they can be used by others in the industry. This work in its current state is not ready for widespread implementation. An examination of a wider set of host–pathogen systems for remote disease assessment is needed and field-based detection in the presence of other abiotic and biotic factors, all of which are essential for the widespread adoption of remote disease detection. Furthermore, the steps and processes used would be best suited as a background language of a web-based platform or software that ran the tasks without the ability of the user to manipulate code.

Conclusions

Classic field scouting techniques for pathogen identification and disease incidence quantification can be subjective and time-consuming. Furthermore, scouting on foot can be destructive to the plant, costly, and burdensome, especially during the rainy season (Barbedo et al. 2016). Traditionally, fungicide application programs treat pathogen pressure with a homogenous pesticide application rather than localized applications based on disease presence (Mahlein et al. 2012; West et al. 2003). Remote sensing techniques can provide an alternative to traditional field sampling, resolving many of these concerns through an objective approach to sampling and provide more insightful integrated pest management programs required for agricultural efficiency in the future.

The potential for the application of remote sensing and machine learning for disease detection was evaluated in these case studies. Based on the results, a simple analysis with various vegetation indices in the broccoli trial revealed areas of poor plant growth but was poorly correlated with disease; instead, fungicide phytotoxic effects were related to areas of poor plant growth and only discernable by conventional on-foot scouting. This indicates limited efficacy of the image analysis to properly categorize the cause of changes in plant health. Alternatively, an SVM model using NDVI and the red band as indicators of disease allowed for accurate detection of black leg on turnip, and remotely sensed data were effectively used to train an SVM using the novel vegetation index, MRMVI, which allowed for detection of gray mold on hemp. While these accomplishments should not be overlooked, the time and resource investment required to successfully develop effective modeling under certain scenarios should be noted. Further research and analysis are necessary to validate the application of these tools in field-based settings and larger regional settings.

The case studies also addressed whether remote sensing and machine learning could be substituted as alternative disease detection methods rather than the traditional field-based technique of scouting on foot. This research found that the gray mold incidence on inflorescences could be quantified with remotely sensed data using an SVM model, but there are limitations to adopting it as a replacement for traditional field scouting on foot. The results indicated that this tool could be used as an alternative to field-based techniques for hemp grown for buds and possibly grain if ranking the order of treatments is prioritized over the true percentage of disease incidence that would be found in the field on foot. In regard to the remote detection of black leg on turnip, the results indicated that increased spatial resolution is needed for field-based applications of remote sensing technology and further model development.

This research builds on recent studies that have successfully used remote sensing with multispectral sensors for the detection of plant disease. All three case studies used various combinations of vegetation indices with an SVM model and in the case of the hemp model, a binary classifier threshold, which is less commonly used but still effective in this case. More current work gravitates toward integrated machine learning and, more recently, deep learning models as both the equipment and analysis options continue to evolve. Flights of hemp fields were effectively conducted at an average elevation comparable to other studies that accomplished disease detection with UAVs, while black leg on turnip detection used lower elevation and likely required an optical sensor/camera with greater spatial resolution for the inclusion of a UAV for disease detection. Future work should demonstrate the application of remote sensing conducted ex situ to facilitate the adoption of these tools by growers and researchers. Furthermore, increasingly higher flight elevations, examinations of a wider set of host–pathogen systems for remote disease assessment, and field-based detection in the presence of other abiotic and biotic factors should be sought after because all are essential to the widespread adoption of remote disease detection.

References cited

Abdulridha J, Ehsani R, Abd-Elrahman A, Ampatzidis Y. 2019. A remote sensing technique for detecting laurel wilt disease in avocado in presence of other biotic and abiotic stresses. Comput Electron Agric. 156:549–557. https://doi.org/10.1016/j.compag.2018.12.018.

Albetis J, Duthoit S, Guttler F, Jacquin A, Goulard M, Poilvé H, Feret J-B, Dedieu G. 2017. Detection of *Flavescence dorée* grapevine disease using Unmanned Aerial Vehicle (UAV) multispectral imagery. Remote Sens. 9(4):308. https://doi.org/10.3390/rs9040308.

Arivazhagan S, Shebiah RN, Ananthi S, Varthini SV. 2013. Detection of unhealthy region of plant leaves and classification of plant leaf diseases using texture features. Agric Eng Int: CIGR J. 15:211–217.

Bates TA. 2021. Science Takes Flight: Detection of Black Leg on Turnip Gray Mold on Hemp. MSc thesis, Oregon State University, Corvallis, OR, USA.

Barbedo JGA. 2013. Digital image processing techniques for detecting, quantifying and classifying plant diseases. SpringerPlus. 2:1–12. https://doi.org/10.1186/2193-1801-2-660.

Barbedo JGA, Koenigkan LV, Santos TT. 2016. Identifying multiple plant diseases using digital image processing. Biosyst. Eng. 147:104–116. https://doi.org/10.1016/j.biosystemseng.2016.03.012.

Behmann J, Steinrücken J, Plümer L. 2014. Detection of early plant stress responses in hyperspectral images. ISPRS J. Photogramm. Remote Sens. 93:98–111. https://doi.org/10.1016/j.isprsjprs.2014.03.016.

Bravo C, Moshou D, West J, McCartney A, Ramon H. 2003. Early disease detection in wheat fields using spectral reflectance. Biosyst Eng. 84(2):137–145. https://doi.org/10.1016/S1537-5110(02)00269-6.

Brecht D. 2018. Remote sensing indices [Blog post]. Medium.com. Retrieved from https://medium.com/regen-network/remote-sensing-indices-389153e3d947.

Broome JC, English JT, Marois JJ, Latorre BA, Aviles JC. 1995. Development of an infection model for Botrytis bunch rot of grapes based on wetness duration and temperature. Phytopathology. 85(1):97–102. https://doi.org/10.1094/Phyto-85-97.

Buckland KR, Rasmussen A, Nackley L. 2020. Unoccupied aerial systems: A guide for finding the right system for your Oregon farm. Oregon State University Extension Publications EM9298, Corvallis, OR, USA.

Bulger MA, Ellis MA, Madden LV. 1987. Influence of temperature and wetness duration on infection of strawberry flowers by *Botrytis cinerea* and disease incidence of fruit originating from infected flowers. Phytopathology. 77(8):1225–1230. https://doi.org/10.1094/Phyto-77-1225.

Candiago S, Remondino F, De Giglio M, Dubbini M, Gattelli M. 2015. Evaluating multispectral images and vegetation indices for precision farming applications from UAV images. Remote Sens. 7(4):4026–4047. https://doi.org/10.3390/rs70404026.

Camargo A, Smith JS. 2009a. Image pattern classification for the identification of disease causing agents in plants. Comput Electron Agric. 66(2):121–125. https://doi.org/10.1016/j.compag.2009.01.003.

Camargo A, Smith JS. 2009b. An image-processing based algorithm to automatically identify plant disease visual symptoms. Biosyst Eng. 102(1):9–21. https://doi.org/10.1016/j.biosystemseng.2008.09.030.

Carisse O. 2016. Epidemiology and aerobiology of *Botrytis* spp, p 127–148. In: Fillinger S, Elad Y (eds). *Botrytis* - the fungus, the pathogen and its management in agricultural systems. Springer, New York, NY, USA. https://doi.org/10.1007/978-3-319-23371-0_7.

Claassen BJ, Berry PA, Thomas WJ, Mallory-Smith C, Ocamb CM. 2021. Black leg and chlorotic leaf spot on Brassicaceae crop and weed hosts in western Oregon. Plant Dis. 105. https://doi.org/10.1094/PDIS-03-21-0665-RE.

Dammer KH, Möller B, Rodemann B, Heppner D. 2011. Detection of head blight (*Fusarium* ssp.) in winter wheat by color and multispectral image analyses. Crop Prot. 30(4):420–428. https://doi.org/10.1016/j.cropro.2010.12.015.

De Kock SL, Holz G. 1992. Blossom-end rot of pears: Systemic infection of flowers and immature fruit by *Botrytis cinerea*. J Phytopathol. 135:317–327. https://doi.org/10.1111/j.1439-0434.1992.tb04317.x.

Fitzgerald G, Rodriguez D, O'Leary G. 2010. Measuring and predicting canopy nitrogen nutrition in wheat using a spectral index—The canopy chlorophyll content index (CCCI). Field Crops Research. 116(3):318–324. https://doi.org/10.1016/j.fcr.2010.01.010.

Ferentinos KP, Barda M, Damer D. 2019. An image-based deep learning model for cannabis diseases, nutrient deficiencies and pests identification, p 134–145. In: Oliveira PM, Novais P, Reis LP (eds). EPIA Conference on Artificial Intelligence pages, Springer, New York, NY, USA. https://doi.org/10.1007/978-3-030-30241-2_12.

Fourie JF, Holz G. 1995. Initial infection processes by *Botrytis cinerea* on nectarine and plum fruit and the development of decay. Phytopathology. 85(1):82–87. https://doi.org/10.1094/Phyto-85-82.

Franke J, Menz G. 2007. Multi-temporal wheat disease detection by multi-spectral remote sensing. Precision Agric. 8(3): 161–172. https://doi.org/10.1007/s11119-007-9036-y.

Hamuda E, Glavin M, Jones E. 2016. A survey of image processing techniques for plant extraction and segmentation in the field. Comput Electron Agric. 125: 184–199. https://doi.org/10.1016/j.compag.2016.04.024.

Heim RH, Wright IJ, Scarth P, Carnegie AJ, Taylor D, Oldeland J. 2019. Multispectral, aerial disease detection for myrtle rust (*Austropuccinia psidii*) on a lemon myrtle plantation. Drones. 3(1):25. https://doi.org/10.3390/drones3010025.

Hsieh TF, Huang JW, Hsiang T. 2001. Light and scanning electron microscopy studies on the infection of oriental lily leaves by *Botrytis elliptica*. Eur J Plant Pathol. 107:571–581. https://doi.org/10.1023/A:1017947328718.

Mahlein AK, Rumpf T, Welke P, Dehne HW, Plümer L, Steiner U, Oerke EC. 2013. Development of spectral indices for detecting and identifying plant diseases. Remote Sens Environ. 128:21–30. https://doi.org/10.1016/j.rse.2012.09.019.

Mahlein AK, Oerke EC, Steiner U, Dehne HW. 2012. Recent advances in sensing plant diseases for precision crop protection. Eur J Plant Pathol. 133:197–209.

Mahlein AK, Steiner U, Dehne HW, Oerke EC. 2010. Spectral signatures of sugar beet leaves for the detection and differentiation of diseases. Precision Agric. 11(4):413–431. https://doi.org/10.1007/s11119-010-9180-7.

Maniruzzaman M, Rahman MJ, Al-MehediHasan M, Suri HS, Abedin MM, El-Baz A, Suri JS. 2018. Accurate diabetes risk stratification using machine learning: role of missing value and outliers. J Med Syst. 42:1–17.

McPartland JM. 1996. A review of Cannabis diseases. J International Hemp Association. 3:19–23.

McPartland JM, Clarke RC, Watson DP. 2000. Hemp diseases and pests: management and biological control. CABI Publishers, New York, NY, USA. https://doi.org/10.1079/9780851994543.0000.

Merz M, Pedro D, Skliros V, Bergenhem C, Himanka M, Houge T, Matos-Carvalho JP, Lundkvist H, Cürüklü B, Hamrén R, Ameri AE, Ahlberg C, Johansen G. 2022. Autonomous UAS-based agriculture applications: General overview and relevant European case studies. Drones. 6(5):128. https://doi.org/10.3390/drones6050128.

Naidu RA, Perry EM, Pierce FJ, Mekuria T. 2009. The potential of spectral reflectance technique for the detection of Grapevine leafroll-associated virus-3 in two red-berried wine grape cultivars. Comput Electron Agric. 66(1):38–45. https://doi.org/10.1016/j.compag.2008.11.007.

Nelson RE. 1951. Factors influencing the infection of table grapes by *Botrytis cinerea*. Phytopathology. 41:319–326.

Neumann M, Hallau L, Klatt B, Kersting K, Bauckhage C. 2014. Erosion band features for cell phone image based plant disease classification, p 3315–3320. In: Proceedings of 22nd International Conference on Pattern Recognition. Stockholm, Sweden. Institute of Electrical and Electronics Engineers (IEEE), Piscataway, NJ, USA.

Ocamb CM, Buckland K, Bates TA. 2019. Evaluation of materials for Alternaria black spot and wirestem of broccoli in Oregon, 2018. Plant Dis Manage Rep. 13:V093.

Pathak H, Kumar G, Mohapatra SD, Gaikwad BB, Rane J. 2020. Use of drones in agriculture: Potentials, Problems and Policy Needs. ICAR-National Institute of Abiotic Stress Management. 300:4–15.

Pettorelli N. 2013. Normalized difference vegetation index. Oxford University Press, Oxford, UK. https://doi.org/10.1093/acprof:osobl/9780199693160.001.0001.

Rumpf T, Mahlein AK, Steiner U, Oerke EC, Dehne HW, Plümer L. 2010. Early detection and classification of plant diseases with support vector machines based on hyperspectral reflectance. Comput Electron Agric. 74(1):91–99. https://doi.org/10.1016/j.compag.2010.06.009.

US Department of Agriculture–National Agricultural Statistics Service. 2023. https://www.nass.usda.gov/Statistics_by_State/Oregon/Publications/Annual_Statistical_Bulletin/2023/OR_ANN_2023.pdf.

West JS, Bravo C, Oberti R, Lemaire D, Moshou D, McCartney HA. 2003. The potential of optical canopy measurement for targeted control of field crop diseases. Annu Rev Phytopathol. 41:593–614. https://doi.org/10.1146/annurev.phyto.41.121702.103726.

Yang CM, Cheng CH, Chen RK. 2007. Changes in spectral characteristics of rice canopy infested with brown planthopper and leaffolder. Crop Sci. 47(1):329–335. https://doi.org/10.2135/cropsci2006.05.0335.

Zhang J, Huang Y, Pu R, Gonzalez-Moreno P, Yuan L, Wu K, Huang W. 2019. Monitoring plant diseases and pests through remote sensing technology: A review. Comput Electron Agric. 165:104943. https://doi.org/10.1016/j.compag.2019.104943.

Zhou R, Kaneko SI, Tanaka F, Kayamori M, Shimizu M. 2014. Disease detection of Cercospora leaf spot in sugar beet by robust template matching. Comput Electron Agric. 108:58–70. https://doi.org/10.1016/j.compag.2014.07.004.